Inorganic Chemistry
Article

Inorg. Chem. **2011**, *50*, 125–135 **125**
DOI: 10.1021/ic101468p

Steric and Electronic Consequences of Flexibility in a Tetradentate Redox-Active Ligand: Ti(IV) and Zr(IV) Complexes

Géza Szigethy and Alan F. Heyduk*

Department of Chemistry, University of California, Irvine, California 92697, United States

Received July 22, 2010

A redox-active, tetradentate ligand, *N,N′*-bis-(3-dimethylamino-propyl)-4,5-dimethoxy-benzene-1,2-diamide ($[N_2N_2^{cat}]^{2-}$), was developed, and the six-coordinate metal complexes $[N_2N_2^{cat}]TiCl_2$ (**3**) and $[N_2N_2^{cat}]ZrCl_2$ (**4**) were synthesized. The tetradentate ligand was determined to be fluxional in **3** and **4**, enabled by reversible dissociation of the neutral amine groups of the $[N_2N_2^{cat}]^{2-}$ ligand. Both amine arms of **3** could be replaced by *N,N*-dimethylaminopyridine with an overall free energy change of $-4.64(3)$ kcal mol^{-1} at 298 K. Cyclic voltammetry experiments were used to probe the redox capabilities of the $[N_2N_2^{cat}]^{2-}$ ligand: complex **3** exhibited two one-electron oxidations at -0.19 and -0.52 V versus $[Cp_2Fe]^{+/0}$ while **4** exhibited a single two-electron oxidation at -0.55 V. Substitution of the chlorides in **3** for an imide afforded the dimer $\{[N_2N_2^{cat}]Ti(\mu\text{-}p\text{-}NC_6H_4Me)\}_2$, in which the metal centers are five-coordinate because of dissociation of one amine arm of the $[N_2N_2^{cat}]^{2-}$ ligand. While the bis-azide complex $[N_2N_2^{cat}]Ti(N_3)_2$ was stable toward elimination of N_2, the bis-phenylacetylide complex $[N_2N_2^{cat}]Ti(C{\equiv}CPh)_2$ could be oxidized by $PhICl_2$, resulting in subsequent reductive elimination of 1,4-diphenylbutadiyne.

Introduction

Variable oxidation states are a key feature of transition-metal catalysts for a wide variety of chemical transformations, the majority of which require the use of catalysts employing relatively expensive 4d and 5d metals (e.g., Pd for Suzuki coupling[1] or Rh for hydrogenation[2]). It has been observed that interactions between redox-active ligands and transition metals can result in the formation of coordination compounds capable of multielectron electron transfer processes, leading to valence tautomerism and redox activity for metal ions that typically do not exhibit reversible, oxidation state changes under mild conditions.[3−13] Using redox-active ligands to impart oxidation state versatility on inexpensive and abundant transition metals is an attractive alternative to the use of platinum group metals in catalytic transformations. With catalyst redox reactivity more dependent on the electronic properties of the ligand than on the metal center, this design strategy allows the choice of transition metal to address other aspects of reactivity such as substrate binding or metal−ligand bond polarization.

Late transition metals exhibit rich redox chemistry when bound to redox-active ligands,[6,14] owing to favorable overlap between the valence orbitals of the metal and the coordinated ligand.[15,16] Because valence electrons can feasibly come from the ligand or the metal center in these metal complexes, assigning formal oxidation states is often difficult leading to the description of non-innocent ligands.[17] To help define the role redox-active ligands can play in the reactivity of transition metal complexes, recent work in our group has focused on characterizing and developing unique reactivity of d^0 transition metal complexes with chelating, redox-active ligands.[8−13] A lack of (formal) metal-based valence electrons in these complexes precludes the possibility of traditional redox reactivity and highlights the redox behavior of the ligands in question

*To whom correspondence should be addressed. E-mail: aheyduk@uci.edu.

(1) Miyaura, N.; Suzuki, A. *Chem. Rev.* **1995**, *95*, 2457–2483.
(2) Tararov, V. I.; Börner, A. *Synlett* **2005**, *2*, 203–211.
(3) Chaudhuri, P.; Hess, M.; Hildenbrand, K.; Bill, E.; Weyhermüller, T.; Wieghardt *Inorg. Chem.* **1999**, *38*, 2781–2790.
(4) Cador, O.; Chaubre, F.; Dei, A.; Sangregorio, C.; Slageren, J. V.; Vaz, M. G. F. *Inorg. Chem.* **2003**, *42*, 6432–6440.
(5) Adams, D. M.; Noodleman, L.; Hendrickson, D. N. *Inorg. Chem.* **1997**, *36*, 3966–3984.
(6) Pierpont, C. G. *Coord. Chem. Rev.* **2001**, *219−221*, 415–433.
(7) Evangelio, E.; Ruiz-Molina, D. *Eur. J. Inorg. Chem.* **2005**, 2957–2971.
(8) Blackmore, K. J.; Lal, N.; Ziller, J. W.; Heyduk, A. F. *Eur. J. Inorg. Chem.* **2009**, 735–743.
(9) Blackmore, K. J.; Sly, M. B.; Haneline, M. R.; Ziller, J. W.; Heyduk, A. F. *Inorg. Chem.* **2008**, *47*, 10522–10532.
(10) Ketterer, N. A.; Fan, H.; Blackmore, K. J.; Yang, X.; Ziller, J. W.; Baik, M.-H.; Heyduk, A. F. *J. Am. Chem. Soc.* **2008**, *130*, 4364–4374.
(11) Nguyen, A. I.; Blackmore, K. J.; Carter, S. M.; Zarkesh, R. A.; Heyduk, A. F. *J. Am. Chem. Soc.* **2009**, *131*, 3307–3316.
(12) Zarkesh, R. A.; Heyduk, A. F. *Organometallics* **2009**, *28*, 6629–6631.
(13) Zarkesh, R. A.; Ziller, J. W.; Heyduk, A. F. *Angew. Chem., Int. Ed.* **2008**, *47*, 4715–4718.
(14) Pierpont, C. G.; Buchanan, R. M. *Coord. Chem. Rev.* **1981**, *38*, 45–87.
(15) Masui, H.; Lever, A. B. P.; Auburn, P. R. *Inorg. Chem.* **1991**, *30*, 2402–2410.
(16) Gorelsky, S. I.; Lever, A. B. P.; Ebadi, M. *Coord. Chem. Rev.* **2002**, *230*, 97–105.
(17) Butin, K. P.; Beloglazkina, E. K.; Zyk, N. V. *Russ. Chem. Rev.* **2005**, *74*, 531–553.

Published on Web 11/30/2010

Scheme 1

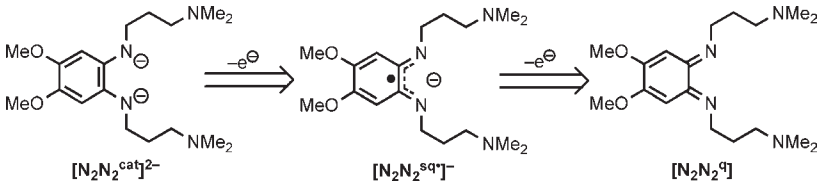

and the reactivity they impart on the metal centers to which they are bound.

A common molecular topology in redox-active ligands is that of catechol, the nitrogen-coordinating *o*-phenylene diamine analogue, or their hybrids.[14] Electron-rich catecholates are employed extensively in nature for their ability to stabilize the ferric cation,[18,19] and their mild redox potentials make them ideal coordination platforms for use as redox-active ligands.[15] Sequential oxidation of a dianionic catecholate ligand leads in a stepwise fashion to a monoanionic, radical semiquinonate followed by a neutral *ortho*-quinone, all of which form five-membered chelate rings when bound to metal ions. The three oxidation states of the catecholate ligand platform differ by small but readily observed changes in intraligand bond distances.[20] While these oxidation state changes do not require significant geometric rearrangement of the ligand, the semiquinonate and quinone oxidation states of the ligand do show decreased metal affinity, occasionally resulting in dissociation of the oxidized ligand from the metal coordination sphere.[9,10,14]

The tetradentate ligand *N,N′*-bis-(3-dimethylamino-propyl)-4,5-dimethoxy-benzene-1,2-diamine ($[N_2N_2^{cat}]H_2$, Scheme 1) was developed as a flexible, redox-active ligand that can stay coordinated to metal ions in all three ligand oxidation states. Designed around an electron-rich *ortho*-phenylenediamine core, $[N_2N_2^{cat}]H_2$ is unique in its inclusion of both flexible alkyl arms containing trialkylamine donors to present four binding sites to a coordinated metal and electron-donating methoxy groups into the phenylene ring to enhance the reducing power of the ligand.[11,21,22] Upon deprotonation, the $[N_2N_2^{cat}]^{2-}$ ligand can undergo two one-electron oxidations to afford semiquinonate, $[N_2N_2^{sq\bullet}]^{-}$, and quinone, $[N_2N_2^{q}]$, oxidation states as shown in Scheme 1. The fully oxidized, $[N_2N_2^{q}]$ form of the ligand is an α-diimine, a class of ligands that readily bind to metal ions across the transition-metal series. A ligand of similar geometry to $[N_2N_2^{cat}]H_2$ but without the donating methoxy groups has been reported.[23] While there was no investigation of ligand-based redox properties, these studies showed that alkyl arms with three methylene units provided the most relaxed molecular geometries upon metal coordination. We report herein the synthesis, characterization, and preliminary reactivity studies of the $[N_2N_2^{cat}]^{2-}$ ligand coordinated to titanium(IV) and zirconium(IV) metal centers.

Experimental Section

General Information. With the exception of **1** and **2**, the compounds described herein are oxygen and moisture sensitive, so manipulations were carried out under a nitrogen or argon atmosphere using standard Schlenk or glovebox techniques. Solvents were purified by sparging with argon followed by sequential passage through activated Q5 and alumina columns to remove oxygen and water, respectively. NMR spectra were collected with Bruker Avance 500 MHz spectrometers (^{1}H 500 MHz, ^{13}C 128 MHz) in either C_6D_6 or $CDCl_3$ solvents that were degassed by several freeze−pump−thaw cycles, dried with sodium benzophenone ketyl radical and CaH_2, respectively, and vacuum-distilled before use. ^{1}H and ^{13}C NMR spectra were referenced to TMS using the residual ^{1}H and ^{13}C impurities in the solvent (7.15 and 128.02 for C_6D_6 and 7.26 and 77.00 for $CDCl_3$, respectively). NMR spectra were measured at 298 K unless otherwise noted, and chemical shifts are reported by using the standard δ notation in parts per million, with splitting patterns indicated as follows: s = singlet, d = doublet, t = triplet, q = quartet, quin. = quintet, br = broad. FTIR spectra were recorded with a Perkin−Elmer Spectrum One spectrophotometer as KBr pellets. UV−visible spectra were recorded with Perkin-Elmer Lambda 800 spectrometer as solutions in dry, degassed benzene or toluene. Electrospray Ionization (ESI) mass spectrometry was performed at the Mass Spectrometry Facility at University of California, Irvine. Chemicals were purchased from commercial sources and used as received with the exception of 4,5-diaminoveratrole,[24] $MCl_4(THF)_2$ (M = Ti, Zr),[25] and $PhICl_2$,[26] which were synthesized following literature procedures from commercially available precursors.

***N,N′*-Bis-(3-chloro-propyl)-4,5-dimethoxy-benzene-1,2-diamide (1).** A biphasic mixture of 4,5-diaminoveratrole (14.6 g, 86.8 mmol) dissolved in 200 mL of degassed CH_2Cl_2 and 400 mL of degassed, 1/2-saturated Na_2CO_3 was vigorously stirred while cooling in an ice bath under argon. To this mixture, 3-chloropropionyl chloride (25.0 mL, 272 mmol) was added over the span of 5 min. The mixture seized with light solids that were broken up, and the mixture was allowed to stir at room temperature overnight. After filtration, the isolated solids were washed with water (2 × 100 mL), Et_2O (2 × 70 mL), then triturated twice with 1:1 Et_2O:$CHCl_3$, once with Et_2O, and dried under vacuum to yield the clean product as a beige powder (28.0 g, 92%). Anal. Calcd. (Found) for $C_{14}H_{18}N_2O_4Cl_2$ (%): C, 48.15 (47.90); H, 5.20 (5.19); N, 8.02 (7.90). ^{1}H NMR ($CDCl_3$): δ 2.81 (t, C*H*$_2$, *J* = 6.5 Hz, 4H), 3.84 (s, C*H*$_3$, 6H), 3.88 (t, C*H*$_2$, *J* = 6.5 Hz, 4H), 6.86 (s, arom. *H*, 2H), 7.92 (s, N*H*, 2H). ^{13}C NMR ($CDCl_3$): δ 39.68 (*C*H$_2$), 40.09 (*C*H$_2$), 56.11 (O−*C*H$_3$), 108.40 (aryl-*C*), 123.06 (aryl-*C*), 147.34 (aryl-*C*), 168.85 (amide-*C*). MS (ESI+): *m*/*z* = 370.98 (MH+), 372.97 (MNa+), 720.96 (M_2H+).

***N,N′*-Bis-(3-dimethylamino-propyl)-4,5-dimethoxy-benzene-1,2-diamide (2). Using $Me_2NH\cdot HCl$.** A heterogeneous mixture of **1** (10.0 g, 28.6 mmol), dimethylamine hydrochloride (5.19 g, 63.6 mmol), and potassium carbonate (12.0 g, 86.5 mmol) was stirred in 170 mL of MeOH overnight at reflux. The mixture was cooled, and the MeOH was removed by rotary evaporator. The residue was stirred in 120 mL of CH_2Cl_2 overnight and filtered, washing the cake several times with CH_2Cl_2. The combined organics were concentrated under vacuum, and the residue was triturated with Et_2O and dried under vacuum to yield product

(18) Raymond, K. N. *Pure Appl. Chem.* **1994**, *66*, 773–781.
(19) Sánchez, P.; Gálvez, N.; Calocio, E.; Minones, E.; Dominguez-Vera, J. M. *Dalton Trans.* **2005**, *4*, 811–813.
(20) Zanello, P.; Corsini, M. *Coord. Chem. Rev.* **2006**, *250*, 2000–2022.
(21) Schrock, R. R.; Lee, J.; Liang, L.-C.; Davis, W. M. *Inorg. Chim. Acta* **1998**, *270*, 353–362.
(22) Lionetti, D.; Medvecz, A. J.; Ugrinova, V.; Quiroz-Guzman, M.; Noll, B. C.; Brown, S. N. *Inorg. Chem.* **2010**, *49*, 4687–4697.
(23) Hahn, F. E.; Wittenbecher, L.; Van, D. L.; Zabula, A. V. *Inorg. Chem.* **2007**, *46*, 7662–7667.
(24) Ottenwaelder, X.; Ruiz-Garcia, R.; Blondin, G.; Carasco, R.; Cano, J.; Lexa, D.; Journaux, Y.; Aukauloo, A. *Chem. Commun.* **2004**, *5*, 504–5.
(25) Manzer, L. E. *Inorg. Synth.* **1982**, *21*, 135–40.
(26) Lucas, H. J.; Kennedy, E. R. *Org. Synth.* **1955**, *3*, 482.

(9.55 g, 91%). ^{1}H NMR ($CDCl_3$): δ 2.32 (s, CH_3, 12H), 2.51 (t, CH_2, J = 6.5 Hz, 4H), 2.66 (t, CH_2, J = 6.5 Hz, 4H), 3.85 (s, CH_3, 6H), 7.00 (s, arom. H, 2H), 9.91 (s, NH, 2H). ^{13}C NMR ($CDCl_3$): δ 33.84 (*C*H_2), 44.87 (N−*C*H_3), 55.19 (*C*H_2), 56.17 (O−*C*H_3), 108.59 (aryl-*C*), 123.73 (aryl-*C*), 146.72 (aryl-*C*), 171.15 (amide-*C*). MS (ESI+): m/z = 367.13 (MH+), 389.13 (MNa+), 733.28 (M_2H+), 755.26 (M_2Na+).

Using Gaseous Me_2NH. A suspension of **1** (10.0 g, 28.6 mmol) was stirred in 150 mL of CH_2Cl_2 at room temperature, through which gaseous Me_2NH was slowly bubbled. When the resultant exotherm brought the solution close to reflux the solution was allowed to cool to room temperature. This process was repeated until thin layer chromatography (TLC) analysis in EtOAc showed only material with R_f = 0. The now homogeneous CH_2Cl_2 solution was washed with 1 M NaOH in 20% saturated NaCl (3 × 100 mL). The combined aqueous layers were extracted with 100 mL of CH_2Cl_2, the combined organics were dried with $MgSO_4$ and the solvent removed under reduced pressure. The residue was co-evaporated twice with Et_2O, resulting in quantitative yield of the product as a beige/brown solid of sufficient purity to be used in subsequent reactions.

***N,N′*-Bis-(3-dimethylamino-propyl)-4,5-dimethoxy-benzene-1, 2-diamine, [$N_2N_2^{cat}$]H_2.** A solution of **2** (6.96 g, 19.0 mmol) dissolved in dry THF was added via cannula to a suspension of $LiAlH_4$ (2.16 g, 57.0 mmol) in 20 mL of dry tetrahydrofuran (THF) cooled in a dry ice/^{i}PrOH bath under argon. After bubbling ceased, the mixture was warmed to room temperature and then maintained at reflux for 9 h to yield a yellow suspension. The mixture was cooled in a dry ice bath, and water (20.0 mL, 1.11 mol) was slowly added to quench the $LiAlH_4$. The mixture was held at reflux overnight and cooled to room temperature. The mixture was filtered through Celite in an argon-filled glovebag, and the solvent was removed from the filtrate using a rotary evaporator. The residue was distilled (0.4 mtor, T > 140 °C) using a kugelrohr to yield a yellow oil (5.80 g, 90%). Anal. Calcd. (Found) for $C_{18}H_{34}N_4O_2$ (%): C, 63.87 (63.73); H, 10.12 (10.56); N, 16.55 (16.30). ^{1}H NMR (C_6D_6): δ1.58 (quin., CH_2, J = 6.5 Hz, 4H), 2.06 (s, CH_3, 12H), 2.18 (t, CH_2, J = 6.5 Hz, 4H), 3.02 (t, CH_2, J = 6.5 Hz, 4H), 3.70 (s, CH_3, 6H), 3.83 (s, br, NH, 2H), 6.55 (s, arom. H, 2H). ^{13}C NMR (C_6D_6): δ 27.60 (*C*H_2), 44.22 (*C*H_2), 45.59 (N−*C*H_3), 58.08 (*C*H_2), 58.49 (O−*C*H_3), 102.82 (aryl-*C*), 133.13 (aryl-*C*), 143.96 (aryl-*C*). MS (ESI+): m/z = 339.17 (MH+), 377.19 (MK+). UV−vis (C_6H_6) λ_{max}/nm (ε/M^{-1} cm^{-1}): 316 (6,100).

General Procedure for Synthesis of [$N_2N_2^{cat}$]$TiCl_2$ (3) and [$N_2N_2^{cat}$]$ZrCl_2$ (4). A solution of [$N_2N_2^{cat}$]H_2 (2.00 g, 5.91 mmol) in 60 mL of Et_2O was frozen in a cold well. Immediately upon thawing, a solution of ^{n}BuLi in hexanes (3.01 M, 3.93 mL, 11.8 mmol) was added, and the resultant suspension was stirred at room temperature for 2 h, during which time the color changed from pale purple to yellow. The solvent volume was reduced to 2 mL under vacuum, and the residue was suspended in 100 mL of toluene and frozen. To this slurry was added $MCl_4(THF)_2$ (1.97 g for M = Ti and 2.23 g for M = Zr, 5.91 mmol), and the mixture was allowed to stir at room temperature for 4 days. The deeply colored suspension was filtered, the toluene removed under vacuum, and the residue was co-evaporated once with pentane yielding clean [N_2N_2]MCl_2 complexes. Samples for crystallographic analysis were grown by cooling of a toluene/cyclopentane solution at −35 °C.

[$N_2N_2^{cat}$]$TiCl_2$ (3). Dark purple, microcrystalline solid (2.26 g, 84%). ^{1}H NMR ($CDCl_3$): δ 2.22 (d, br, CH_2, J = 14.0 Hz, 2H), 2.36 (q, br, CH_2, J = 14.5 Hz, 2H), 2.83 (s, CH_3, 6H), 2.94 (s, CH_3, 6H), 3.02 (d, br, CH_2, 12.5 Hz, 2H), 3.57 (d, br, CH_2, J=12.5 Hz, 2H), 3.71 (s, CH_3, 6H), 4.29 (t, br, CH_2, J=12.5 Hz, 2H), 5.48−5.54 (m, br, arom. H + CH_2, 4H). ^{13}C NMR ($CDCl_3$): δ 27.71 (*C*H_2), 52.94 (*C*H_2), 56.12 (N−*C*H_3), 65.77 (O−*C*H_3), 91.81 (aryl-*C*), 139.27 (aryl-*C*), 147.08 (aryl-*C*). UV−vis (toluene) λ_{max}/nm (ε/M^{-1} cm^{-1}): 332 (5,400), 412 (10,400), 554 (1,700).

[$N_2N_2^{cat}$]$ZrCl_2$ (4). Dark red/brown amorphous solid (2.68 g, 91%). Anal. Calcd. (Found) for $C_{18}H_{32}N_4O_2Cl_2Zr$ (%): C, 43.36 (43.79); H, 6.47 (6.23); N, 11.24 (11.04). ^{1}H NMR (CD_2Cl_2, 253 K): δ 1.84 (d, br, CH_2, J = 11.5 Hz, 2H), 2.00 (q, br, CH_2, J = 13.5 Hz, 2H), 2.37 (s, CH_2, 6H), 2.66 (d, br, CH_2, J = 12.5 Hz, 2H), 2.86 (s, CH_3, 6H), 3.68 (s, br, CH_2, 2H), 3.80 (s, CH_3, 6H), 3.87 (d, br, CH_2, J = 13.5 Hz, 2H), 4.48 (t, br, CH_2, J = 13.0 Hz, 2H), 6.13 (s, arom. H, 2H). ^{13}C NMR ($CDCl_3$): δ 25.97 (*C*H_2), 49.19 (*C*H_2), 57.25 (N−CH_3), 65.68 (O−*C*H_3), 94.36 (aryl-*C*), 141.10 (aryl-*C*), 142.25 (aryl-*C*). UV−vis (toluene) λ_{max}/nm (ε/M^{-1} cm^{-1}): 304 (15,000), 356 (6,000).

General Procedure for Synthesis of [$N_2N_2^{cat}$]$Ti(NMe_2)_2$ (5) and [$N_2N_2^{cat}$]$Zr(NMe_2)_2$ (6). A barely thawed solution of [$N_2N_2^{cat}$]-MCl_2 [M = Ti (**3**), Zr (**4**)] (0.44−0.50 mmol, 1 equiv.) in 10 mL of toluene was added to a barely thawed suspension of $LiNMe_2$ (2 equiv) in 7 mL of Et_2O and stirred at room temperature overnight. The reaction mixture was filtered, and the solvent was removed under vacuum and co-evaporated twice with pentane yielding the [$N_2N_2^{cat}$]M(NMe_2)$_2$ complexes.

[$N_2N_2^{cat}$]$Ti(NMe_2)_2$ (5). Tacky, dark purple semi-solid, 88%. ^{1}H NMR (C_6D_6): δ 1.74 (quin., CH_2, J = 6.5 Hz, 4H), 1.95 (s, CH_3, 12H), 2.19 (t, CH_3, J = 6.5 Hz, 4H), 2.97 (s, CH_3, 12H), 3.81 (t, CH_3, J = 6.5 Hz, 4H), 3.91 (s, CH_3, 6H), 6.48 (s, arom. H, 2H). ^{13}C NMR (C_6D_6): δ 28.80 (*C*H_2), 45.30 (N−*C*H_3), 47.53 (N−*C*H_3), 51.61 (*C*H_2), 59.12 (*C*H_2), 60.89 (O−*C*H_3), 95.93 (aryl-*C*), 128.31 (aryl-*C*), 143.18 (aryl-*C*). UV−vis (toluene) λ_{max}/nm (ε/M^{-1} cm^{-1}): 322 (11,100), 382 (9,000), 538 (3,500).

[$N_2N_2^{cat}$]$Zr(NMe_2)_2$ (6). Yellow solid, 86%. ^{1}H NMR (C_6D_6): δ 1.54 (s, br, CH_2, 4H), 1.88 (s, CH_3, 12H), 2.19 (t, CH_3, J = 5.5 Hz, 4H), 3.92−3.94 (m, CH_3 + CH_2, 10H), 6.52 (s, arom. H, 2H). ^{13}C NMR (C_6D_6): δ 25.88 (*C*H_2), 44.08 (N−*C*H_3), 47.67 (N−*C*H_3), 47.77 (*C*H_2), 59.46 (*C*H_2), 65.53 (O−*C*H_3), 96.01 (aryl-*C*), 128.31 (aryl-*C*), 145.04 (aryl-*C*). UV−vis (toluene) λ_{max}/nm (ε/M^{-1} cm^{-1}): 370 (11,400).

{[$N_2N_2^{cat}$]$Ti(\mu\text{-}p\text{-}NC_6H_4Me)$}$_2$ (7). *p*-Toluidine (118 mg, 1.10 mmol) and KH (44.1 mg, 1.10 mmol) were combined in cold THF and stirred at room temperature until the mixture was homogeneous and no more bubbling was observed. This THF solution was cooled in a cold well until nearly frozen, then KH (44.1 mg, 1.10 mmol) and a cold solution of **3** (500 mg, 1.10 mmol) in THF were added, with a final solution volume of 50 mL. This mixture was warmed to room temperature and then refluxed overnight under argon, during which time an inky-brown color developed. Upon cooling to room temperature, the THF was removed under vacuum, and the residue was extracted into 50 mL of toluene and filtered. The solvent was removed from the filtrate, and the residue was co-evaporated twice with pentane to yield a brown/black, amorphous solid. This solid was dissolved in a minimum amount of THF, then diluted with pentane and held at −35 °C overnight. The resultant brown/black powder was filtered and dried, yielding the clean product (349 mg, 65%). ^{1}H NMR (C_6D_6): δ 1.54 (s, br, CH_2, 2H), 2.01−2.20 (m, br, CH_2 + CH_3, 21H), 3.84 (s, CH_3, 6H), 4.69 (s, br, CH_2, 4H), 6.19 (s, arom. H, 1H), 6.56 (s, arom. H, 1H), 6.78 (d, arom. H, J = 8.5 Hz, 2H), 6.97 (d, arom. H, J = 6.5 Hz, 2H). ^{13}C NMR (C_6D_6): δ 20.76 (*C*H_3), 26.30 (*C*H_2), 28.73 (*C*H_2), 46.09 (N−*C*H_3), 48.98 (*C*H_2), 49.00 (*C*H_2), 55.98 (*C*H_2), 56.00 (N−*C*H_3), 58.37 (*C*H_2), 58.54 (*C*H_2), 65.06 (O−*C*H_3), 67.80 (O−*C*H_3), 96.85 (aryl-*C*), 97.17 (aryl-*C*), 121.28 (aryl-*C*), 128.84 (aryl-*C*), 129.54 (aryl-*C*), 141.80 (aryl-*C*), 141.84 (aryl-*C*), 141.98 (aryl-*C*), 144.517 (aryl-*C*), 144.90 (aryl-*C*), 159.56 (aryl-*C*). UV−vis (C_6H_6) λ_{max}/nm (ε/M^{-1} cm^{-1}): 322 (22,000), 404 (16,800), 444 (15,800).

[$N_2N_2^{cat}$]$Ti(N_3)_2$, (8). A mixture of **3** (200 mg, 0.439 mmol) and NaN_3 (62.8 mg, 0.966 mmol) was stirred in 15 mL of THF at room temperature for 5 days. The solution was filtered, and solvent was removed under vacuum. The residue was stirred in 10 mL of toluene, filtered, and the solvent was removed from the filtrate under vacuum to yield a purple, microcrystalline solid

(171 mg, 83%). Samples for analysis and X-ray diffraction analysis were recrystallized from a toluene/cyclopentane mixture at −35 °C. ^{1}H NMR ($CDCl_3$): δ 2.15 (d, br, CH_2, J = 13.5 Hz, 2H), 2.29 (q, br, 17.5 Hz, 2.67 (s, CH_3, 12H), 2.92 (t, br, CH_2, 12.5 Hz, 2H), 3.67 (d, br, CH_2, J = 12.5 Hz, 2H), 3.72 (s, CH_3, 6H), 3.79 (t, br, CH_2, J = 12.5 Hz, 2H), 4.82 (t, br, CH_2, J = 12.5 Hz, 2H), 5.61 (s, arom. H, 2H). ^{13}C NMR ($CDCl_3$): δ 27.89 (*C*H$_2$), 46.82 (N−*C*H$_3$), 50.74 (*C*H$_2$), 53.27 (N−*C*H$_3$), 56.28 (*C*H$_2$), 65.25 (O−*C*H$_3$), 91.72 (aryl-*C*), 139.60 (aryl-*C*), 146.13 (aryl-*C*). FTIR: 2089 cm^{-1} (N_3). UV−vis (toluene) λ_{max}/nm (ε/M^{-1} cm^{-1}): 330 (9,400), 416 (15,600), 564 (3,600).

[$N_2N_2^{cat}$]Ti(C≡CPh)$_2$ (9). To a solution of phenylacetylene (156 mg, 1.52 mmol) in 10 mL of THF was added sodium metal (35.0 mg, 1.52 mmol), and the mixture was stirred vigorously overnight, resulting in a white suspension of the sodium phenylacetylide salt. This suspension was frozen, and upon barely thawing was combined with a cold solution of **3** (346 mg, 0.761 mmol) in THF, with a final reaction volume of 45 mL. The mixture was stirred for 2 days at room temperature, followed by removal of the THF under vacuum. The residue was stirred in 40 mL of toluene, filtered, and the solvent was removed under vacuum, and the residue co-evaporated twice with pentane to yield the residue as a black/brown solid (352 mg, 79%). Anal. Calcd. (Found) for $C_{34}H_{42}N_4O_2Ti$ (%): C, 69.62 (69.25); H, 7.22 (7.21); N, 9.55 (9.61). ^{1}H NMR ($CDCl_3$, 218 K): δ 2.16 (d, br, CH_2, J = 13.0 Hz, 2H), 2.37 (d, br, CH_2, J = 16.0 Hz, 2H), 2.78 (s, CH_3, 6H), 3.02 (d, br, 12.0 Hz, 2H), 3.17 (s, CH_3, 6H), 3.63 (d, br, CH_2, J = 11.0 Hz, 2H), 3.74 (s, CH_3, 6H), 4.54 (t, br, CH_2, J = 12.0 Hz, 2H), 5.63 (s, arom. H, 2H), 5.69 (t, br, CH_2, J = 12.5 Hz, 2H), 7.21 (t, arom. H, J = 7.0 Hz, 2H), 7.24−7.27 (m, arom. H, 4H), 7.36 (d, arom. H, J = 7.0 Hz, 4H). ^{13}C NMR ($CDCl_3$): δ 28.14 (*C*H$_2$), 51.66 (*C*H$_2$), 56.44 (N−*C*H$_3$), 66.02 (O−*C*H$_3$), 91.71 (alkyne-*C*), 101.204 (alkyne-*C*), 125.55 (aryl-*C*), 126.36 (aryl-*C*), 128.02 (aryl-*C*), 131.22 (aryl-*C*), 140.98 (aryl-*C*), 145.01 (aryl-*C*), 155.54 (aryl-*C*). FTIR: 2063 cm^{-1} (C≡C). UV−vis (C_6H_6) λ_{max}/nm (ε/M^{-1} cm^{-1}): 336 (11,800), 422 (10,400), 542 (2,900).

Oxidation of 9 by $PhICl_2$. Upon partial thawing of a frozen solution of **9** (100 mg, 0.170 mmol) in 18 mL of Et_2O, $PhICl_2$ (46.9 mg, 0.170 mmol) was added, and the mixture was stirred overnight at room temperature, resulting in the precipitation of a dark, microcrystalline solid in a dark purple solution. Solvent was removed under vacuum, yielding a crude residue weighing 104 mg, and whose NMR in C_6D_6 indicated the presence only of **3** and a new aryl-containing product. The residue was dissolved in 10 mL of THF and passed through three successive pipet columns of silica gel. The resulting pale yellow eluent was held under vacuum, yielding 16.4 mg of residue, which NMR analysis in $CDCl_3$ indicated was clean 1,4-diphenylbutadiyne by comparison to a reference spectrum (48%).

Electrochemical Methods. Electrochemical experiments were performed on a Gamry Series G 300 Potentiostat/Galvanostat/ZRA (Gamry Instruments, Warminster, PA, U.S.A.) using a 3.0 mm glassy carbon working electrode, a platinum wire auxiliary electrode, and a silver wire reference electrode. Electrochemical experiments were performed at ambient temperature (20−24 °C), either in a nitrogen-filled glovebox or were under an atmosphere of argon. Tetrabutylammonium hexafluorophosphate (Acros) was recrystallized from ethanol three times and dried under vacuum before use. Sample concentrations were 1.0 mM in THF with 0.10 M [NBu_4][PF_6] as the supporting electrolyte. All potentials are referenced to [Cp_2Fe]$^{+/0}$,[27] using [Cp_2Co][PF_6] as an internal standard (−1.34 V vs [Cp_2Fe]$^{+/0}$).

X-ray Diffraction. X-ray diffraction data were collected on crystals mounted on glass fibers using a Bruker CCD platform diffractometer equipped with a CCD detector. Measurements were carried out using Mo K_α (λ = 0.71073 Å) radiation, which was wavelength selected with a single-crystal graphite monochromator. A full sphere of data was collected for each crystal structure. The APEX2 program package was used to determine unit-cell parameters and to collect data.[28] The raw frame data were processed sing SAINT[29] and SADABS[30] to yield the reflection data files. Subsequent calculations were carried out using the SHELXTL[31] program suite. Structures were solved by direct methods and refined on F^2 by full-matrix least-squares techniques to convergence. Analytical scattering factors for neutral atoms were used throughout the analyses.[32] Hydrogen atoms, though visible in the difference Fourier map, were generated at calculated positions, and their positions refined using the riding model. ORTEP diagrams were generated using ORTEP-3[33] for Windows, and all thermal ellipsoids are drawn at the 50% probability level. Diffraction collection and refinement data are shown in Table 1.

[$N_2N_2^{cat}$]$TiCl_2$ (3). A complete sphere of diffraction data was collected on a red crystal of approximate dimensions 0.251 × 0.221 × 0.069 mm using a 25 s/frame scan time. The diffraction symmetry was 2/*m* and the systematic absences were consistent with the monoclinic space group $P2_1/c$ that was later determined to be correct.

[$N_2N_2^{cat}$]$ZrCl_2$ (4). A complete sphere of diffraction data was collected on a red plate of dimensions 0.23 × 0.19 × 0.13 mm using a 20 s/frame scan time. The diffraction symmetry was *mmm*, and the systematic absences were consistent with the monoclinic space group $P2_12_12_1$ that was later determined to be correct. The presence of only one enantiomer of **4** in the crystal structure is assumed to be a solid state phenomenon, as there should be no driving force to form either the Δ or the Λ enantiomer in bulk solution with the symmetric $(N_2N_2)^{2-}$ ligand.

[$N_2N_2^{cat}$]Ti(N_3)$_2$ (7). A complete sphere of diffraction data was collected on a red plate of dimensions 0.206 × 0.157 × 0.057 mm using a 40 s/frame scan time. The diffraction symmetry was $\bar{1}$, and the systematic absences were consistent with the triclinic space group $P\bar{1}$ that was later determined to be correct. Positional disorder was observed in the positions of two methylene carbons in one of the ligand chelate arms. These carbon atoms were disordered over two positions whose occupancies were freely refined to a 90:10 occupancy ratio. The other ligand chelate arm exhibits relatively elongated thermal ellipsoids consistent with a libration disorder. Modeling this chelate arm as positional disorder over two positions resulted in unstable refinement and required an excessive amount of refinement constraints, so the thermal ellipsoids were left unmodeled.

{[$N_2N_2^{cat}$]Ti(μ-p-NC_6H_4Me)}$_2$ (9). A complete sphere of diffraction data was collected on a red plate of dimensions 0.352 × 0.165 × 0.074 mm using a 30 s/frame scan time. The diffraction symmetry was 2/*m*, and the systematic absences were consistent with the monoclinic space group $P2_1/n$ that was later determined to be correct. One methoxy group on the ligand displayed positional disorder so was modeled over two positions with a freely refined occupancy ratio of 66:34. Standard distance restraints were used in the modeling of this fragment.

Results and Discussion

Ligand Synthesis and Metalation. Synthesis of [$N_2N_2^{cat}$]H_2 proceeded in a similar fashion to that described for a structurally analogous compound.[23] Following the readily

(27) Connelly, N. G.; Geiger, W. E. *Chem. Rev.* **1996**, *96*, 877–910.

(28) *APEX2*, Version 2008.3−0, or Version 2.2−0; Bruker AXS, Inc.: Madison, WI, 2007.

(29) *SAINT*, Version 7.53a (or 7.46a); Bruker AXS, Inc.: Madison, WI, 2007.

(30) Sheldrick, G. M. *SADABS*, Version 2007/4; Bruker AXS, Inc: Madison, WI, 2007.

(31) Sheldrick, G. M. *SHELXTL*, Version 6.12; Bruker AXS, Inc: Madison, WI, 2001.

(32) *International Tables for X-Ray Crystallography*; Kluwer Academic Publishers: Dordrecht, The Netherlands, 1992; Vol. *C*.

(33) Farrugia, L. J. *J. Appl. Crystallogr.* **1997**, *30*, 565.

Table 1. X-ray Data Collection and Refinement Parameters

	$[N_2N_2^{cat}]TiCl_2$ (**3**)	$[N_2N_2^{cat}]ZrCl_2$ (**4**)	$\{[N_2N_2^{cat}]Ti(\mu\text{-}p\text{-}NC_6H_4Me)\}_2$ (**7**)	$[N_2N_2^{cat}]Ti(N_3)_2$ (**8**)
empirical formula	$C_{18}H_{32}N_4O_2Cl_2Ti$	$C_{18}H_{32}N_4O_2Cl_2Zr$	$C_{50}H_{78}N_{10}O_4Ti_2$	$C_{18}H_{32}N_{10}O_2Ti$
formula weight	455.28	498.60	979.02	468.44
crystal system	monoclinic	orthorhombic	monoclinic	triclinic
space group	$P2_1/c$	$P2_12_12_1$	$P2_1/n$	$P\bar{1}$
T [K]	148(2)	153(2)	149(2)	152(2)
a [Å]	11.1199(6)	8.0438(4)	11.1838(6)	9.6998(7)
b [Å]	8.6895(4)	10.2298(5)	10.1818(6)	10.7251(7)
c [Å]	22.5886(11)	27.4376(14)	22.1409(12)	11.5990(8)
α [deg]	90	90	90	80.3700(10)
β [deg]	103.1270(10)	90	94.5520(10)	76.5230(10)
γ [deg]	90	90	90	72.1880(10)
V [Å^3]	2125.62(18)	2257.7(2)	2513.3(2)	1111.16(13)
Z	4	4	2	2
refl collected	23794	26229	27948	13392
data/restr/param	5011/0/246	5364/0/247	5914/10/321	5302/0/291
R_1 [$I > 2\sigma(I)$][a]	0.0337	0.0166	0.0365	0.0470
wR_2(all data)[a]	0.0873	0.0439	0.1011	0.1165
GOF[a]	1.026	1.077	1.033	1.052

[a] $R_1 = \sum||F_o| - |F_c||/\sum|F_o|$; $wR_2 = [\sum w(F_o^2 - F_c^2)^2/\sum w(F_o^2)^2]^{1/2}$; GOF $= [\sum w(|F_o| - |F_c|)^2/(n-m)]^{1/2}$.

Scheme 2[a]

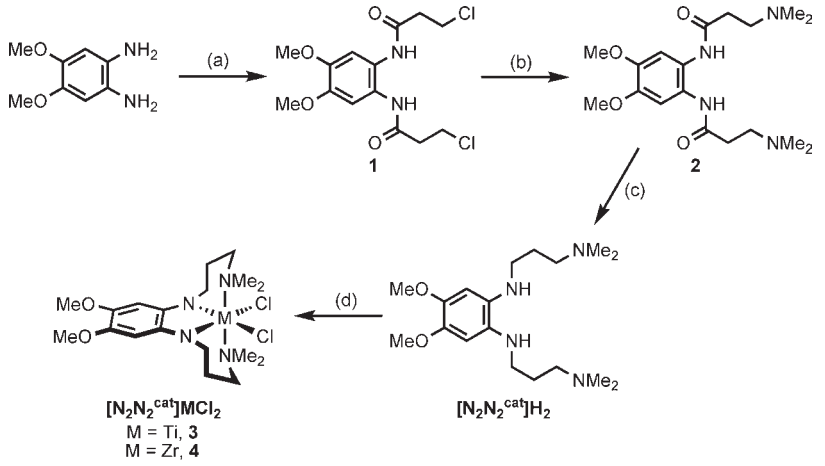

[a] **(a) 3-chloropropionyl chloride, Na_2CO_3; (b) $Me_2NH\cdot HCl$, K_2CO_3; (c) $LiAlH_4$; (d) ^{n}BuLi, $MCl_4(THF)_2$, M = Ti(IV), Zr(IV).**

scaleable process illustrated in Scheme 2, reaction of freshly reduced 4,5-diaminoveratrole with 3-chloropropionyl chloride afforded the air stable dichloride **1** in 92% yield. Reaction of **1** with dimethylammonium chloride and potassium carbonate afforded the bis-dimethylamine **2** in excellent yield. Upon reduction of **2** with lithium aluminum hydride, $[N_2N_2^{cat}]H_2$ was distilled as a yellow, oxygen-sensitive oil that is stable at room temperature under an inert atmosphere.

Metalation of $[N_2N_2^{cat}]H_2$ proceeded in good yields via in situ generation of $[N_2N_2^{cat}]Li_2$ using $[N_2N_2^{cat}]H_2$ and *n*-butyllithium, followed by treatment with $MCl_4(THF)_2$ salts (M = Ti, Zr) in toluene. Because of the heterogeneity of the reaction and the potential for coordination oligomer formation, metalation reactions were stirred for several days. After filtration and solvent removal, $[N_2N_2^{cat}]TiCl_2$ (**3**) and $[N_2N_2^{cat}]ZrCl_2$ (**4**) were obtained as dark purple and dark red microcrystalline solids, respectively.

The colors of **3** and **4** relative to free $[N_2N_2^{cat}]H_2$ indicate the emergence of low-energy charge-transfer transitions in the metalated complexes. The UV−visible spectra of **3** and **4** are compared against that of $[N_2N_2^{cat}]H_2$ in Figure 1. Free $[N_2N_2^{cat}]H_2$ exhibits only a single strong absorbance at 316 nm which barely tails into the visible region of the spectrum,

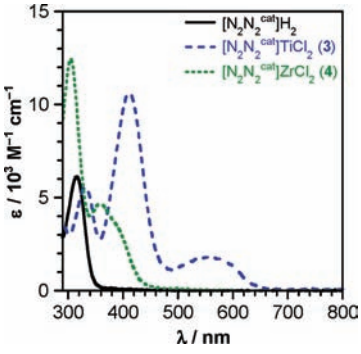

Figure 1. UV−visible spectra of $[N_2N_2^{cat}]H_2$ (solid black), $[N_2N_2^{cat}]TiCl_2$ (**3**, dashed blue), and $[N_2N_2^{cat}]ZrCl_2$ (**4**, dotted green) taken in toluene (**3** and **4**) and benzene ($[N_2N_2^{cat}]H_2$).

consistent with the pale yellow color of the free ligand. This transition blue shifts to 304 nm and gains considerable intensity upon coordination of the ligand to zirconium in **4**, which also displays multiple charge-transfer bands in the 350−400 nm range. The UV−vis absorbance spectrum of **3** is profoundly different from that of **4**. A high-energy band is still observed at 332 nm in addition to a strong charge transfer

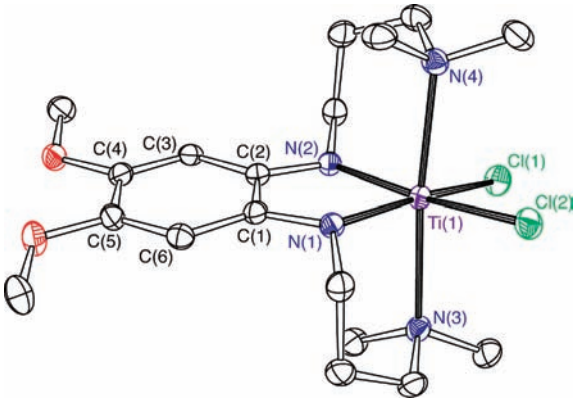

Figure 2. Crystal structure of $[N_2N_2^{cat}]TiCl_2$ **3**. Thermal ellipsoids are drawn at the 50% probability level.

Table 2. Selected Metric Parameters for $[N_2N_2^{cat}]TiCl_2$ (**3**), $[N_2N_2^{cat}]ZrCl_2$ (**4**), and $[N_2N_2^{cat}]Ti(N_3)_2$ (**8**)

	$[N_2N_2^{cat}]$-$TiCl_2$ **3**	$[N_2N_2^{cat}]$-$ZrCl_2$ **4**	$[N_2N_2^{cat}]$-$Ti(N_3)_2$ **8**
	Bond Lengths [Å]		
C(1)−C(2)	1.408(2)	1.4082(18)	1.411(3)
C(1)−N(1)	1.389(2)	1.4015(17)	1.388(2)
C(2)−N(2)	1.387(2)	1.4006(17)	1.389(3)
M(1)−N(1)	1.9838(14)	2.0985(12)	1.9779(16)
M(1)−N(2)	1.9812(14)	2.0896(11)	1.9820(19)
M(1)−N(3)	2.3138(15)	2.4220(12)	2.277(2)
M(1)−N(4)	2.3365(15)	2.3991(12)	2.302(2)
M(1)−Cl(1)	2.3919(5)	2.4977(4)	
M(1)−Cl(2)	2.3818(5)	2.4894(4)	
Ti(1)−N(5)			2.077(2)
Ti(1)−N(8)			2.0311(19)
	Bond Angles [deg]		
N(1)−M(1)−N(2)	78.00(6)	74.30(4)	77.45(7)
N(1)−M(1)−N(3)	82.04(6)	81.24(4)	85.24(7)
N(1)−M(1)−N(4)	101.33(6)	109.79(4)	103.24(7)
N(2)−M(1)−N(3)	102.13(6)	108.02(4)	102.91(9)
N(2)−M(1)−N(4)	83.14(6)	83.16(4)	83.33(9)
N(3)−M(1)−N(4)	174.31(5)	166.44(4)	170.51(7)
Ti(1)−N(5)−N(6)			158.9(2)
Ti(1)−N(8)−N(9)			155.81(17)

transition at 412 nm and multiple weaker transitions in the 500−600 nm envelope. The appearance of intense low-energy transitions upon metalation of $[N_2N_2^{cat}]H_2$, and the blue-shift of these transitions upon dropping from titanium to zirconium, is consistent with their assignment as ligand-to-metal charge-transfer (LMCT) transitions originating on the electron rich $[N_2N_2^{cat}]^{2-}$ ligand to the electrophilic d^0 titanium and zirconium metal centers of **3** and **4**, respectively.

The coordination geometries of **3** and **4** were probed by single-crystal X-ray diffraction techniques and were revealed to be monomeric six-coordinate species. The crystal structure of **3** is shown in Figure 2; zirconium complex **4** is analogous (see Supporting Information, Figure S1). Selected metrical data for both **3** and **4** are listed in Table 2. Both complexes are pseudo-octahedral with the neutral amine donors located trans to one another. A non-crystallographic, molecular C_2 axis bisects the cis Cl−M−Cl and N_{aryl}−M−N_{aryl} angles. The metal−ligand bond distances in **3** and **4** are consistent with other group IV metal-amide, -amine, and -chloride bond distances[10,34] and support the assignment of **3** and **4** as titanium(IV) and zirconium(IV) complexes, respectively. Equivalent M−X (X = N, Cl) bond distances within each complex vary by a maximum of 0.02 Å, indicating a symmetrically coordinated metal center. The M−N(1) and M−N(2) bond distances are comparable to monodentate anilide complexes.[35−39] Additional support for the M^{IV} and $[N_2N_2^{cat}]^{2-}$ ligand oxidation state assignments are the C−C and C−N distances within the phenylenediamide unit, which are consistent with other C_{aryl}−C_{aryl} and C_{aryl}−N(sp^2) bond distances in uncoordinated aryl-amines.[40]

The major differences between the structures of **3** and **4** lie in the bond angles generated by coordination of the $[N_2N_2^{cat}]^{2-}$ ligand to the metal centers, highlighting the size difference between the titanium and zirconium ions. The N_{alkyl}−M−N_{alkyl} angle in **3** is close to linear at 174° but in **4** this angle closes to 166°, indicating that the zirconium ion does not sit as deeply in the $[N_2N_2^{cat}]^{2-}$ binding pocket. The strain of the $[N_2N_2^{cat}]^{2-}$ ligand upon coordination is further highlighted by the N_{amide}−M−N_{alkyl} bond angles, which range from 83° to 102° in **3** and from 82° to 109° in **4**. Finally the twist angle between the planes defined by the N(1)−M−N(2) and Cl(1)−M−Cl(2) atom groups should be 0° in an ideal octahedron; however, the geometric strain imposed by the arms of the $[N_2N_2]^{2-}$ ligand result in twist angles of 13.2° in **3** and 22.0° in **4**. While the $[N_2N_2]^{2-}$ ligand readily coordinates both titanium and zirconium ions, the deviations from ideal octahedral coordination geometry suggest that the three methylene units of the amine arms are not quite long enough to satisfy a regular octahedral coordination for zirconium though the smaller titanium is better stabilized (Δr_{ion} = 0.18 Å).[41]

It was expected that the three methylene units of the amine arms would be long enough to accommodate octahedral coordination in **3** and **4**; however, the hybridization adopted by the aryl amine nitrogens N(1) and N(2) in the $[N_2N_2^{cat}]^{2-}$ ligand effectively shorten the reach of the amine arms. The N(1) and N(2) nitrogens are formally sp^2 hybridized eneamines with bond angles ranging between 115° and 123° in **3** and **4**. This hybridization orients the first methylene carbon in the ligand arm equatorially, while a formally sp^3 nitrogen hybridization would allow orientation of the methylene carbon toward the axial coordination position, in turn leading to a more relaxed coordination geometry about the metal center. The consequence of this effect becomes more pronounced as metal size increases, which in turn explains the progressive departure from ideal octahedral geometry observed between structures of **3** and **4** despite linker arms containing three methylene groups.

The NMR spectra of **3** and **4** are consistent with the C_2 symmetry observed in the solid-state structures. Sharp,

(34) Tabernero, V.; Cuenca, T.; Herdtweck *Eur. J. Inorg. Chem.* **2004**, 3154–3162.
(35) Edema, J. J. H.; Duchateau, R.; Gambarotta, S.; Bensimon, C. *Inorg. Chem.* **1991**, *30*, 3585–3587.
(36) Bashall, A.; Collier, P. E.; Gade, L. H.; McPartlin, M.; Mountford, P.; Pugh, S. M.; Radojevic, S.; Schubart, M.; Scowen, I. J.; Trösch, D. J. M. *Organometallics* **2000**, *19*, 4784–4794.
(37) Breen, T. L.; Stephan, D. W. *Organometallics* **1996**, *15*, 4223–4227.
(38) LoCoco, M. D.; Zhang, X.; Jordan, R. F. *J. Am. Chem. Soc.* **2004**, *126*, 15231–15244.
(39) Grigsby, W. J.; Olmstead, M. M.; Power, P. P. *J. Organomet. Chem.* **1996**, *513*, 173–180.
(40) Allen, F. H.; Kennard, O.; Watson, D. G.; Brammer, L.; Orpen, A. G.; Taylor, R. *J. Chem. Soc. Dalton Trans. II* **1987**, S1–S19.
(41) Emsley, J. *The Elements*, 3rd ed.; Clarendon Press: Oxford, 1998.

Scheme 3

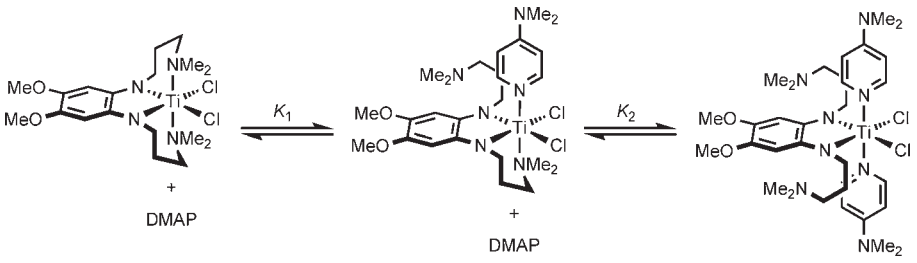

symmetric signals for the aromatic and methoxy protons of the $[N_2N_2^{cat}]^{2-}$ ligands were observed in the ^{1}H NMR spectra of **3** and **4**. The chemical shifts for ligand proton resonances in **3** are generally shifted downfield from the similar resonances in **4**, with the extreme case being one methylene resonance located in a multiplet shared by the aromatic proton in **3** (5.48−5.54 ppm), while the similar resonance in **4** is located at 4.48 ppm. The difference in chemical shift can be attributed to the greater electronegativity of titanium compared to zirconium.

At room temperature, the methylene resonances of the amine arms of both **3** and **4** are split into diastereotopic pairs, and similarly, the N-methyl protons appear as two distinct singlets. The diastereotopic resonances for the amine arms indicate that in solution the chirality of **3** and **4** is preserved on the NMR time scale at 298 K; however, whereas the methylene resonances in **3** exhibit discernible two-bond *J*-coupling patterns at room temperature, those in **4** show significant line broadening, suggesting that an exchange process is occurring slowly. This exchange is also evident in the N-methyl resonances of **4**, which are relatively broad. At elevated temperatures the ^{1}H NMR spectrum of **4** is simplified, with the methylene and N-methyl resonances coalescing to give a single set of peaks. This coalescence is consistent with loss of chirality in **4** via dissociation of an amine arm and rearrangement of the corresponding five-coordinate species. Coalescence temperatures for the methylene proton resonances of **4** could not be determined accurately because of overlapping signals, but the N-methyl proton signals of **4** coalesce at approximately 313 K. Similarly, dynamic behavior was observed in the methylene resonances of **3**, with the N-methyl proton signals coalescing at 328 K. These coalescence temperatures correspond to free energies of activation ($\Delta G^{\ddagger}$) of 16.2(1) kcal·mol^{-1} for **3** and 14.4(1) kcal·mol^{-1} for **4**. The lower $\Delta G^{\ddagger}$ for **4** provides further evidence that the $[N_2N_2^{cat}]^{2-}$ ligand is better suited for stabilizing the smaller titanium ion than the larger zirconium ion.

Ligand Substitution Reactivity of 3. The fluxionality of the amine arms in **3** and **4** suggested that dissociation of an arm could be an effective mechanism for substrate binding at the metal center, prompting a study of the thermodynamics of ligand exchange. Complexes **3** and **4** were exposed to a variety of mono- and bidentate neutral ligands including pyridine, bipyridine, Et_3N, TMEDA, *tert*-butylisonitrile, and Et_3P. Addition of two- to fourfold excesses of these ligands to solutions of **3** or **4** in benzene or chloroform resulted in no change to the ^{1}H NMR resonances of either complex; however, the more nucleophilic 4-dimethylaminopyridine (DMAP) resulted in changes to the NMR spectrum consistent with DMAP coordination to the metal center. The ^{1}H NMR spectrum of **3** with added DMAP shows the unsubstituted, as well as the mono- and disubstituted species, consistent with the equilibrium shown in Scheme 3, and the formation of these adducts is accompanied by the development of a green color in solution. NMR analysis of the DMAP equilibrium with **3** at 298 K in C_6D_6 revealed a K_1 of 99(4) and a K_2 of 25(1), corresponding to ΔG values of −2.72(2) kcal·mol^{-1} and −1.91(1) kcal·mol^{-1} for the stepwise formation of **3**(DMAP) and **3**(DMAP)$_2$ complexes, respectively.

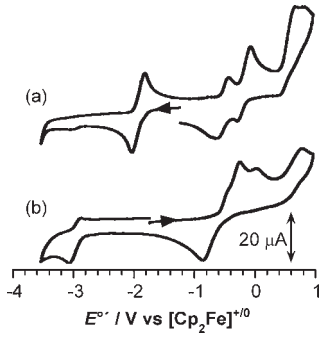

Figure 3. Cyclic voltammograms for (a) $[N_2N_2^{cat}]TiCl_2$ (**3**) and (b) $[N_2N_2^{cat}]ZrCl_2$ (**4**). Spectra were recorded at a 1 mM analyte concentration in 0.1 M $[NBu_4][PF_6]$ in dry, degassed, THF under a nitrogen atmosphere using a 3 mm glassy carbon working electrode, Pt counter electrode, and $Ag^{+/0}$ reference, at 27 °C with a 200 mV/s scan rate.

Table 3. Reduction Potentials of **3** and **4** in 0.1 M $[NBu_4][PF_6]$ in THF

	$E^{o\prime}$/V vs $[Cp_2Fe]^{+/0}$	
	$[N_2N_2^{cat}]TiCl_2$ **3**	$[N_2N_2^{cat}]ZrCl_2$ **4**
E_1		−2.97[a]
E_2	−1.89	
E_3	−0.52	overlapping with
E_4	−0.19	$E_{1/2}$ = −0.55
E_5	0.69[b]	0.77[b]

[a] Irreversible process (E_{pc}). [b] Irreversible process (E_{pa}).

Electrochemistry of 3 and 4. The redox behavior of the $[N_2N_2^{cat}]^{2-}$ ligand in **3** and **4** was probed using cyclic voltammetry, the results of which are shown in Figure 3. Formal potentials referenced against the $[Cp_2Fe]^{+/0}$ redox couple[27] are given in Table 3. Complex **3** displays a reversible one-electron process at −1.89 V, assigned as the $Ti^{IV/III}$ reduction. Two partially reversible one-electron events at −0.52 and −0.19 V are likely the stepwise oxidation of the $[N_2N_2^{cat}]^{2-}$ ligand first to the $[N_2N_2^{sq\bullet}]^{-}$ and then to the $[N_2N_2^{q}]$ oxidation state. An irreversible oxidation event is visible near the edge of the solvent window at 0.69 V and appears to contain two broad features.

The cyclic voltammogram of **4** is simplified relative to that of **3**. First, the process attributable to the $Ti^{IV/III}$ redox

Scheme 4

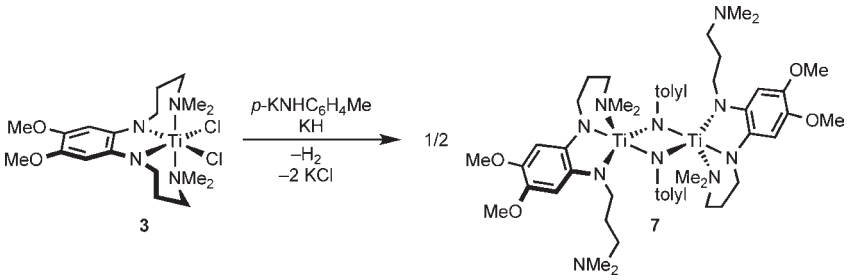

couple of **3** is missing from the voltammogram of **4**. Two irreversible electron transfer events are observed for **4** near the reductive and oxidative edges of the solvent window: an irreversible oxidation at about 0.77 V, and an irreversible reduction at −2.97 V. The redox events associated with the $[N_2N_2^{cat}]^{2-}$ ligand appear as a complex, broad, three-featured peak with an anodic maximum at −0.23 V and a cathodic return wave minimum at −0.87 V. That **3** can undergo stepwise, one-electron oxidations, while **4** appears to be oxidized in a more complicated two-electron process, is indicative of different degrees of interaction between the metal and ligand valence orbitals. Attempts to prepare $[\mathbf{3}]^-$ and $[\mathbf{3}]^+$ for EPR spectroscopic studies to further elucidate metal−ligand electronic interactions were unsuccessful since the desired products could not be isolated cleanly nor characterized definitively.

Metathesis Reactivity with Primary and Secondary Amides. Different M−X functionalities could be introduced to the metal centers of **3** and **4** through metathesis reactions. Reaction of **3** or **4** with lithium alkoxides, organolithium, or Grignard reagents resulted in the formation of multiple products, some of which were insoluble in non-polar organic solvents. Given the propensity of group IV metals to form anionic complexes with anionic ligands,[42] we suspected that incomplete LiCl precipitation was leading to the formation of mixed "-ate" complexes that impeded formation of a single metal product. The exception to this trend were salt metatheses with $LiNMe_2$, which resulted in the formation of the bis-dimethylamide complexes $[N_2N_2^{cat}]Ti(NMe_2)_2$ (**5**) and $[N_2N_2^{cat}]Zr(NMe_2)_2$ (**6**). Titanium complex **5** is a glassy purple residue, while zirconium complex **6** is an amorphous, yellow solid. The ^1H NMR spectra of both complexes at 298 K revealed no diastereotopic splitting of the methylene or N-methyl resonances at room temperature; instead they were coalesced into three broad methylene signals and one sharp dimethylamine signal. These signals were also shifted upfield compared to the corresponding resonances in **3** and **4**. Together these data indicate more rapid ligand arm fluxuation in **5** and **6**, likely caused by both increased steric and electronic saturation at the metal center imparted by the dimethylamide ligands.

Aryl imide dimers of titanium were accessible from **3** through metathesis and deprotonation steps. To avoid complications encountered with lithium salt metatheses, potassium salts were used to prepare the imido complexes. Thus, the reaction of **3** with 1 equiv of potassium *p*-tolyl anilide and 1 equiv of KH led to the formation of a dimeric titanium imido complex, $\{[N_2N_2^{cat}]Ti(\mu\text{-}p\text{-}NC_6H_4Me)\}_2$ (**7**) in high yield as shown in Scheme 4. The dimeric nature of **7** was revealed by single-crystal X-ray diffraction experiments; selected metrical parameters for **7** are listed in Table 4. As shown in Figure 4, the bimetallic core of **7** is bridged by two *p*-tolyl imide ligands. The $[N_2N_2^{cat}]^{2-}$ ligand occupies only three coordination sites on each metal with one amine arm of each ligand unbound. The dimer shows crystallographically

(42) Greenwood, N. N.; Earnshaw, A. *Chemistry of the Elements*; Pergamon Press: New York, 1997.

Table 4. Selected Bond Distances and Angles in the Structure of **7**

Bond Lengths [Å]	
C(1)−C(2)	1.409(2)
C(1)−N(1)	1.384(2)
C(2)−N(2)	1.397(2)
Ti(1)−N(1)	1.9998(14)
Ti(1)−N(2)	1.9980(14)
Ti(1)−N(3)	2.2648(14)
Ti(1)−N(5)	1.9829(14)
Ti(1)−N(5′)	1.9455(14)
Bond Angles [deg]	
N(1) −Ti(1)−N(2)	78.84(6)
N(1)−Ti(1)−N(3)	84.62(5)
N(1)−Ti(1)−N(5)	95.88(6)
N(1)−Ti(1)−N(5′)	177.24(6)
N(2)−Ti(1)−N(3)	125.08(5)
N(2)−Ti(1)−N(5)	115.09(6)
N(2)−Ti(1)−N(5′)	102.82(6)
N(3)−Ti(1)−N(5)	118.50(6)
N(3)−Ti(1)−N(5′)	92.62(5)
N(5)−Ti(1)−N(5′)	85.43(6)

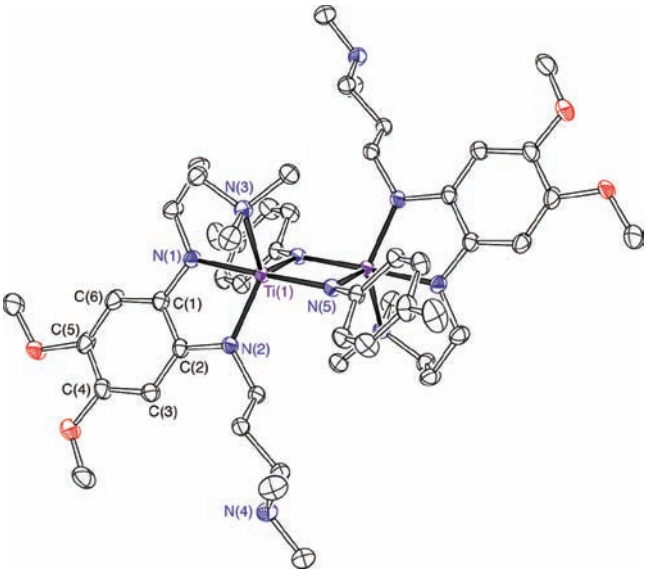

Figure 4. Crystal structure of $\{[N_2N_2^{cat}]Ti(\mu\text{-}p\text{-}NC_6H_4Me)\}_2$ (**7**). Thermal ellipsoids are drawn at the 50% probability level.

Scheme 5

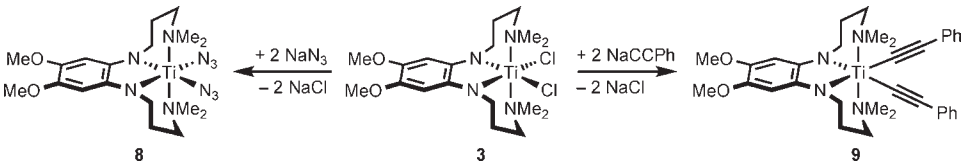

imposed symmetry with an inversion center located at the center of the Ti_2N_2 diamond core. The titanium centers adopt a distorted trigonal bipyramidal coordination geometry, with the amide donors of the $[N_2N_2^{cat}]^{2-}$ ligand occupying one axial [N(1)] and one equatorial [N(2)] coordination site having a bite angle of 79°. The other axial position and a second equatorial position are occupied by the bridging imido nitrogen atoms [N(5)], while the final equatorial position is occupied by one of the amine donors [N(3)] of the $[N_2N_2^{cat}]^{2-}$ ligand. The angle between the axial amide and imide donor atoms is close to ideal at 177°, while the equatorial N−Ti−N angles deviate at most 5° from the ideal 120°. The titanium-amide bond distances associated with the $[N_2N_2^{cat}]^{2-}$ ligand are consistent with those in **3**, indicating there is no abnormal strain placed upon the ligand by displacement of one chelating arm. The axial titanium-imide bond distance is elongated relative to the equatorial titanium-imide bond distance, though both values fall within the range observed for symmetric titanium-imido dimers [1.91(1) Å to 2.05(2) Å],[39] indicating that the difference in bond length is due to the coordination geometry around each metal.

The solution phase ^{1}H NMR data of **7** at room temperature is consistent with the dimeric structure shown in Figure 4. The aryl proton resonances for the $[N_2N_2^{cat}]^{2-}$ ligand appear as two broad singlets separated by 0.37 ppm, indicating inequivalent chemical environments related by a slow exchange process. The signals from the ligand methylene protons are also broadened and appear upfield of 3 ppm, in contrast to the relatively sharp, downfield-shifted methylene resonances observed in **3**. Additionally, the N-methyl proton resonances are already coalesced into a broad singlet at room temperature. These characteristics indicate that the ligand arms in **7** are very fluxional, and rapidly exchange between metal-bound and uncoordinated conformations suggesting the intermediacy of a complex with six-coordinate titanium centers and fully coordinated $[N_2N_2^{cat}]^{2-}$ ligands.

Synthesis of $[N_2N_2^{cat}]Ti(N_3)_2$ (8). Azide metathesis reactions provide a route to the synthesis of titanium azides with the $[N_2N_2^{cat}]^{2-}$ ligand. While the reaction of zirconium complex **4** with sodium azide led to decomposition of the $[N_2N_2^{cat}]Zr$ platform, titanium complex **3** reacted with 2 equiv of sodium azide to afford the titanium bis(azide) complex $[N_2N_2^{cat}]Ti(N_3)_2$ (**8**) in high yields (Scheme 5). In the presence of less than 2 equiv of azide, or at short reaction times, both the mono- and disubstituted titanium products could be observed by NMR spectroscopy; however, these products could not be separated. Complete conversion to bis-azide complex **8** was achieved after 5 days at room temperature with two or more equivalents of NaN_3. The structure of **8**, as determined by single-crystal X-ray diffraction, is illustrated in Figure 5, with selected metrics listed in Table 2. The titanium-amide bonds to the $[N_2N_2^{cat}]^{2-}$ ligand of **8** are within 0.02 Å of those in **3**, and the titanium-amine bonds are elongated by only 0.06 Å. As shown in Table 2,

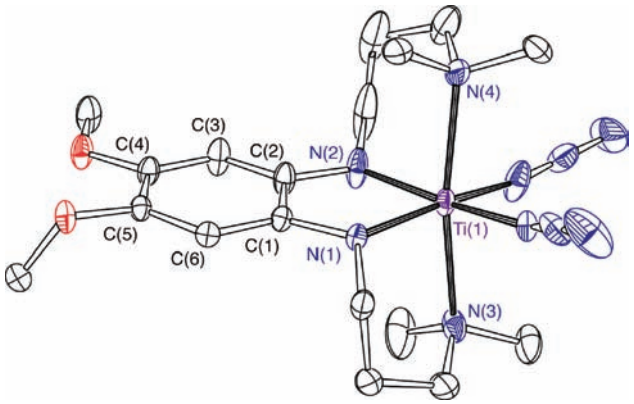

Figure 5. Crystal structure of $[N_2N_2^{cat}]Ti(N_3)_2$ (**8**). Thermal ellipsoids are drawn at the 50% probability level.

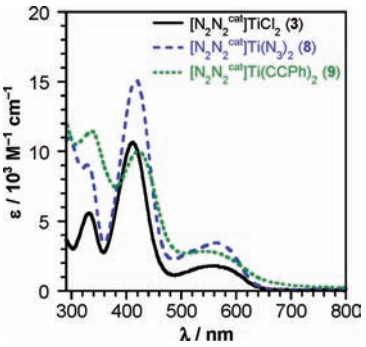

Figure 6. UV−visible spectra of $[N_2N_2^{cat}]TiCl_2$ (**3**, solid black, toluene), $[N_2N_2^{cat}]Ti(N_3)_2$ (**8**, dashed blue, C_6H_6), and $[N_2N_2^{cat}]Ti(C{\equiv}CPh)_2$ (**9**, dotted green, C_6H_6).

all other metrical parameters about the $[N_2N_2^{cat}]Ti$ core are similar for **3** and **8**, consistent with the azide ligands of **8** acting as simple pseudo halides. The azide ligands have a bent end-on coordination mode with Ti(1)−N(5)−N(6) and Ti(1)−N(8)−N(9) angles of 159° and 156°, respectively. The Ti−N_{azide} bond distances average 2.05(2) Å, which is statistically identical to the 2.03(1) Å Ti−N_{azide} bond distances in $Cp_2Ti(N_3)_2$;[43] similarly, the N−N bond distances within the azide ligands are consistent with those observed in other titanium(IV) azide complexes.[43,44]

Solution spectroscopic data also indicates that the redox-active $[N_2N_2^{cat}]Ti$ fragment does not show non-innocent behavior in bis(azide) **8**. The IR-active azide stretch was observed at 2089 cm^{-1}, which is significantly higher than the titanium *trans*-bis(azide), $(bpy)Ti(N_3)_2(NMe_2)_2$ (2080 cm^{-1})[45] and is very similar to the azide

(43) De Gil, E. R.; De Burguera, M.; Rivera, A. V. *Acta Crystallogr.* **1977**, *B33*, 578–579.
(44) Shekar, S.; Twamley, B.; Wehmschulte, R. J. *Inorg. Chem.* **2008**, *47*, 10804–10806.
(45) Carmalt, C. J.; Whaley, S. R.; Lall, P. S.; Cowley, A. H.; Jones, R. A.; McBurnett, B. G.; Ekerdt, J. G. *J. Chem. Soc., Dalton Trans.* **1998**, 553–557.

Scheme 6

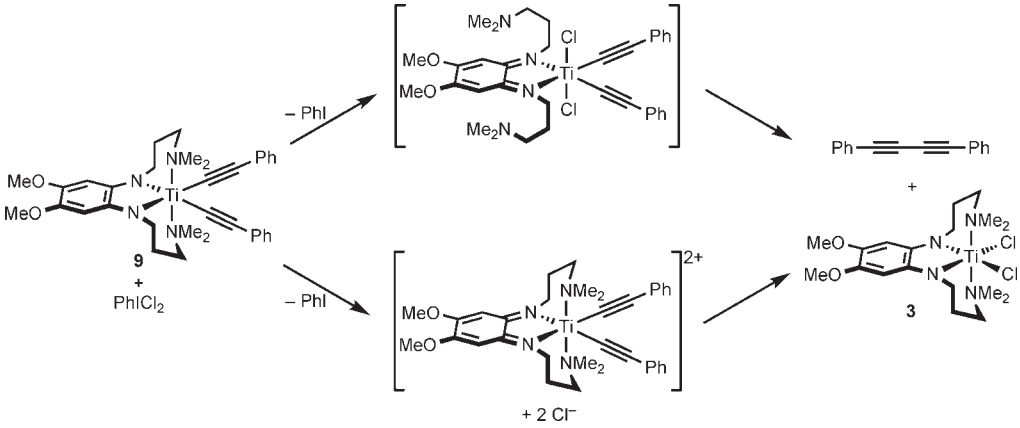

stretch observed for the electrophilic four-coordinate complex $Ti(O^iPr)_3(N_3)$ (2090 cm^{-1}).[46] As shown in Figure 6, the UV−visible absorption spectra of **8** shows minor changes in extinction coefficient relative to **3**, with the energies of all absorption band maxima located within 10 nm of those for **3**. The similarity in the spectra of **3** and **8** would suggest that there is no photoinduced electron transfer to the azide ligands (ligand-to-ligand charge transfer). Consistent with this observation, visible irradiation of **8** did not lead to measurable N_2 expulsion nor formation of a titanium nitride complex. Similarly, prolonged heating of **8** at 100 °C did not result in any measurable formation of a titanium nitride.

Alkyne Coupling with $[N_2N_2^{cat}]Ti(C{\equiv}CPh)_2$. Despite the propensity for **3** and **4** to form intractable solids upon reaction with metal alkyls and metal aryls, exposure of **3** to sodium phenylacetylide cleanly yields the dark brown diacetylide complex $[N_2N_2^{cat}]Ti(C{\equiv}CPh)_2$ (**9**, Scheme 5). The room temperature ^1H NMR spectrum of **9** contains only one very broad resonance for the N-methyl protons, with methylene resonances broadened into the baseline, indicating the amine arms of the $[N_2N_2^{cat}]^{2-}$ ligand to be far more labile than in **3** or **8**. The coalescence temperature for the *N*-methyl proton resonances of **8** is 253 K in $CDCl_3$, and further cooling to 213 K is required to distinguish the diastereotopic methylene proton resonances of **9**. At low temperatures, the methylene protons adopt very similar chemical shifts to those observed in **3**, with the farthest downfield methylene resonance located at 5.69 ppm, about 0.2 ppm downfield of that in **3**. The diastereotopic splitting of the methylene and *N*-methyl protons are consistent with C_2 molecular symmetry in solution as observed for **3**. Because the phenylacetylide ligands should present a similar steric demand to the azides in **8**, the high lability of the ligand arms in **9** arises from the increased σ-donating ability of the sp-hybridized carbon donors of the acetylide ligands.

Solution spectroscopic studies of **9** suggest some electronic coupling between the $[N_2N_2^{cat}]^{2-}$ ligand and the acetylide ligands. Notably small red-shifts were observed in the two high-energy electronic transitions of **9** relative to those of **3** and **8** (Figure 6). In the IR spectrum of **9** the C≡C stretch is observed at 2063 cm^{-1}, which is significantly lower than other titanium(IV) mono- and bis-phenylacetylides.[47−50] These reference complexes all contain cyclopentadienide-based ligands; thus, the formally 16-electron complexes $Cp_2Ti(C{\equiv}CPh)_2$,[49] $Cp^*_2Ti(C{\equiv}CPh)_2$,[48] and $(C_5H_4SiMe_3)_2Ti(C{\equiv}CPh)_2$[50] exhibit C≡C stretches 3−7 cm^{-1} higher than in **9**. The formally 12-electron complex, $(MeC_5H_4)Ti(NMe_2)_2(C{\equiv}CPh)$,[47] (or a 16-electron complex taking into account π-donation from the dimethylamide ligands) exhibits an alkyne stretch 17 cm^{-1} higher than in **9**. That the alkyne stretch appears at lower energy in **9** than in formally 16-electron titanium bis-acetylides indicates a degree of electronic communication between the redox-active orbitals of the $[N_2N_2^{cat}]^{2-}$ ligand and the acetylide ligands, suggesting the possibility of redox-based reactivity for **9**.

Treatment of **9** with 1 equiv of the chlorine surrogate $PhICl_2$ resulted in clean production of 1,4-diphenylbutadiyne and generation of **3**. Oxidative coupling of alkynes typically involves the use of palladium or copper salts, and can even be performed using Grignard reagents and TEMPO as oxidant.[51] To our knowledge the only acetylide coupling that utilizes titanium bis(acetylide) complexes was reported by Wakatsuki et al.,[52] and was enabled by oxidation of terminal ferrocenyl or ruthenocenyl groups attached to the acetylide ligands. The use of halogens to oxidize titanium complexes with normal acetylide ligands led to the elimination of the halo-alkyne (X−C≡CR, X = Cl, Br) in addition to the formation of titanium-halide bonds.[53] In the case of **9**, halogen reagents can oxidize the redox-active ligand to afford a putative $[N_2N_2^q]Ti$ species that could then undergo a subsequent carbon−carbon bond-forming reductive elimination. Scheme 6 shows two potential pathways to the observed butadiyne product. In the upper pathway, oxidative addition of chlorine to **9** would afford a neutral $[N_2N_2^q]TiCl_2(C{\equiv}CPh)_2$ intermediate that could then reductively eliminate butadiyne with recoordination of the amine arms of the $[N_2N_2]$ ligand. Alternatively, an

(46) Schekar, S.; Twamley, B.; Wehmschulte, R. J. *Inorg. Chem.* **2008**, *47*, 10804–10806.
(47) Jenkins, A. D.; Lappert, M. F.; Srivastava, R. C. *J. Organomet. Chem.* **1970**, *23*, 165–172.
(48) Kirchbauer, F. G.; Pellny, P.-M.; Sun, H.; Burlakov, V. V.; Arndt, P.; Baumann, W.; Spannenberg, A.; Rosenthal, U. *Organometallics* **2001**, *20*, 5289–5296.
(49) Köpf, H.; Schmidt, M. *J. Organomet. Chem.* **1967**, *10*, 383–384.
(50) Back, S.; Stein, T.; Frosch, W.; Wu, I.-Y.; Kralik, J.; Büchner, M.; Huttner, G.; Rheinwald, G.; Lang, H. *Inorg. Chim. Acta* **2001**, *325*, 94–102.
(51) Maji, M. S.; Studer, A. *Synthesis* **2009**, *14*, 2467–2470.
(52) Hayashi, Y.; Osawa, M.; Wakatsuki, Y. *J. Organomet. Chem.* **1997**, *542*, 241–246.
(53) Lang, H.; Seyferth, D. *Z. Naturforsch., B: Chem. Sci.* **1990**, *45*, 212–220.

outer-sphere oxidation of **9** by chlorine would afford a dicationic $[N_2N_2^q]Ti(C{\equiv}CPh)_2^{2+}$ intermediate that could reductively eliminate butadiyne upon coordination of chloride formed during the oxidation reaction. The proposed carbon−carbon bond-forming reductive elimination reaction is exactly analogous to the reductive elimination of biphenyl observed for zirconium complexes with redox-active amidophenolate ligands,[54] excepting that both oxidizing equivalents are contained within a single ligand.

Conclusions

The incorporation of neutral amine donor arms into a redox-active phenylenediamide ligand was pursued to circumvent problems associated with metal dissociation upon oxidation of the ligand platform. A potential drawback of this strategy is the generation of coordinatively saturated metal complexes in which the $[N_2N_2^{cat}]^{2-}$ ligand occupies four of six metal coordination sites. In this regard, the combination of neutral amine arms and electrophilic metal ions are well-matched in that reversible amine arm dissociation appears to be both thermodynamically accessible and kinetically facile. Thus the amine arms of the $[N_2N_2^{cat}]^{2-}$ ligand can be viewed as hemilabile ligands[55,56] that serve to protect the metal center and give isolable compounds, yet under reaction conditions dissociate to provide reactive sites in the metal coordination sphere. Ongoing efforts seek to engage both the two-electron reactivity and the hemilabile character of $[N_2N_2^{cat}]M$ fragments in small-molecule activation reactions.

Acknowledgment. The authors thank the UCI Physical Science Center for Solar Energy for supporting this work. A.F.H. is an Alfred P. Sloan Foundation Fellow and a Camille Dreyfus Teacher-Scholar.

Supporting Information Available: Crystallographic information files for reported X-ray structures, crystallographic figures of **4**, and ^1H NMR spectra for all new complexes. This material is available free of charge via the Internet at http://pubs.acs.org.

(54) Haneline, M. R.; Heyduk, A. F. *J. Am. Chem. Soc.* **2006**, *128*, 8410–8411.
(55) Charette, A. B.; Côté, A.; Desrosiers, J.-N.; Bonnaventure, I.; Lindsay, V. N. G.; Lauzon, C.; Tannous, J.; Boezio, A. A. *Pure Appl. Chem.* **2008**, *80*, 881–890.
(56) Faller, J. W.; Grimmond, B. J.; D'Alliessi, D. G. *J. Am. Chem. Soc.* **2001**, *123*, 2525–2529.